Geothermics 86 (2020) 101831

Contents lists available at ScienceDirect

Geothermics

journal homepage: www.elsevier.com/locate/geothermics

An embedded 3D fracture modeling approach for simulating fracture-dominated fluid flow and heat transfer in geothermal reservoirs

Cong Wang[a,b], Philip Winterfeld[a], Bud Johnston[c], Yu-Shu Wu[a,*]

[a] Colorado School of Mines, Golden, USA
[b] Saudi Aramco, Dhahran, Saudi Arabia
[c] National Renewable Energy Laboratory (NREL), Golden, USA

ARTICLE INFO

Keywords:
Geothermal reservoir
Reservoir simulation
Fracture simulation
EDFM

ABSTRACT

In this paper, we describe an efficient modeling approach, named embedded discrete fracture method (EDFM), for incorporating arbitrary 3D, discrete fractures, such as hydraulic fractures or faults, into modeling fracture-dominated fluid flow and heat transfer in fractured geothermal reservoirs. This technique allows 3D discrete fractures to be discretized independently from surrounding rock volume and inserted explicitly into a primary fracture/matrix grid, generated without including 3D discrete fractures in prior. An effective computational algorithm is developed to discretize these 3D discrete fractures and construct local connections between 3D fractures and fracture/matrix grid blocks representing the surrounding rock volume. The constructed gridding information on 3D fractures is then added to the primary grid. This embedded fracture modeling approach can be directly implemented into a developed geothermal reservoir simulator via the integral finite difference (IFD) method or with TOUGH2 technology. This embedded fracture modeling approach is very promising and computationally efficient to handle realistic 3D discrete fractures with complicated geometries, connections, and spatial distributions. Compared with other fracture modeling approaches, it avoids cumbersome 3D unstructured, local refining procedures, and increases computational efficiency by simplifying Jacobian matrix size and sparsity, while maintaining enough accuracy. Several numeral simulations are presented to demonstrate the utility and robustness of the proposed technique. Our numerical experiments show that this approach captures all the key patterns about fluid flow and heat transfer dominated by fractures in these cases. Thus, this approach is readily available to the simulation of fractured geothermal reservoirs with both artificial and natural fractures.

1. Introduction

Geothermal energy is a clean and sustainable energy source, which deals with the heat energy generated and stored within the earth. It includes three major types: the hydrothermal source, the geo-pressured source, and sources stored in hot, dry rocks. The third type has a promising size of the resources, though its commercial development is limited with the currently available technology. These systems are fluid independent, which involve non-porous and impermeable rocks where the temperature is high enough to be useful. The essential step to develop this system is creating a fracture system (either by hydraulic fracturing to create new fractures over a very short period or by the shear reactivation of pre-existing fracture at relatively low pressure just high enough to cause shear failure over a long-time period), and then completing a circulation loop by drilling another well that intersects the hydraulic fracture region. Freshwater is injected from one well, forcing it to flow through the fracture, and then is produced from the other well. In this process, the thermal energy is extracted by the heat conduction when the water is exposed to hot rock surfaces.

Reservoir simulation provides a practical approach to characterize key reservoir parameters in this process (such as temperature, permeability, thermal and hydrologic structures), improve our understandings of such geothermal reservoirs, and evaluate/optimize geothermal utilization scheme. Reservoir simulators are built based on sound physical laws about fluid flow and heat transfer and employ mathematical and numerical techniques to quantify these phenomena. Currently, there are several geothermal simulators available to simulate the complicated coupling process between mass and energy transport in a geothermal reservoir, such as SHAFT79 (Pruess and Schroeder, 1980), MULKOM (Pruess and Wu, 1988), TOUGH2 (Pruess et al., 1999), TAURUS (Settari and Walters, 2001), STARS (Computer Modeling Group Ltd, 2012), ECLIPSE (SCHLUMBERGER, 2009), and INTERSECT

* Corresponding author.
E-mail address: ywu@mines.edu (Y.-S. Wu).

https://doi.org/10.1016/j.geothermics.2020.101831
Received 26 September 2019; Received in revised form 30 December 2019; Accepted 25 February 2020
Available online 29 February 2020

(DeBaun et al., 2005), etc. The simulations studied here were carried out with TOUGH2-EGS (Fakcharoenphol et al., 2013), which belongs to the TOUGH2 family and can simulate the coupled thermal-hydraulic-mechanical-chemical (THMC) process.

For the simulation of hot, dry rock geothermal reservoirs, the key is handling the 2D fluid flow and heat transfer within the large-scale hydraulic fractures, which is coupled to the transient heat conduction equation for surrounding rocks. Traditional modeling techniques to quantify fluid flow and heat transfer with fractures can be divided into two major categories. The first one is the multiple-continua method. Classical double-porosity, double-permeability, multiple interacting continua method (MINC), and multi-subregion upscaling (MSR) all belong in this category (Warren and Root, 1963; Kazemi, 1969; Duguid and Lee, 1977; Pruess et al., 1999; Karimi-Fard et al., 2006; Wu et al., 2007; Hui et al., 2018). In this approach, fracture and matrix are conceptualized as two independent continua, which are overlaid with each other. The fracture continua can exist either locally or globally, depending on reservoir geological conditions. Local interactions between the fracture and matrix are captured by the analytical solution based on the pseudo-steady state assumption or by the numerical upscaling. This numerical approach is effective in simulating natural fractured reservoirs (NFR) in which the number of natural fractures is too large to be handled explicitly. Its state-of-the-art development and industry applications involve waterflooding, sour gas injection, and primary production of a gas condensate (Hui et al., 2008; Gong et al., 2008; Hui et al., 2018). Speedups of two orders of magnitude can be achieved with negligible overall errors for these industry applications. However, this approach has limitations for reservoir simulations with dominant fractures whose length scales are much larger than the grid block size, e.g., hydraulic fractures in shale gas/oil reservoir or hot-dry rock geothermal reservoirs.

The second approach is the explicit fracture modeling. The first technique is using structured grids, in which fractures are represented by a series of small-scale grids (Slough et al., 1999; Sadrpanah et al., 2006). This technique could only model fractures with regular shape and with directions along the principal axis. The second technique is using unstructured grids. The unstructured grids are constructed in a way that grid edges/faces coincide with the fracture (Karimi-Fard et al., 2003; Sun and Schechter, 2014). This technique is general, but constructing such unstructured grids is cumbersome, especially for complicated fractures in three dimensions.

The embedded fracture modeling approach is promising and computationally efficient to handle realistic discrete fractures with complicated geometries and connections. Compared with other methods, it avoids cumbersome unstructured, local refining procedures and increases computational efficiency, while keeps enough accuracy. The concept of EDFM is first introduced by Lee et al. (Lee et al., 2001) to simulate long fractures in a hierarchical fracture model. Like the extended finite element method (X-FEM) for the fracture-related solid deformation analysis (Moës et al., 1999), the EDFM virtually embeds fractures into the original grids for fracture-related fluid flow/heat transfer simulation. Interactions between fracture and local matrix blocks are approximated by analytical solutions. In this way, fractures can be represented independently of the mesh, and so unstructured grids or re-meshing is unnecessary. Though the idea of EDFM seems simple and straightforward, there remain several challenges for its practical deployment for industry applications. First, the accuracy of EDFM is not unconditionally guaranteed because of the above-mentioned local approximation. Wang et al. conducted series of numerical validation tests and observed a discrepancy from analytical solutions for some extreme cases in which the transient-state flow lasts long (i.e., large-size matrix blocks with extremely low diffusivity coefficient) (Wang, 2018). Tene et al. developed a projection-based EDFM to address the accuracy issue as well. They investigated the sensitivity of pEDFM to the position of highly conductive fractures and introduced additional non-neighboring connections between fracture and matrix grid cells to accommodate to low-dimensional structural features (Ţene et al., 2017). Secondly, extending the EDFM from 2D (or 2.5D) to 3D fracture modeling is necessary as realistic large-scale fractures cannot be simply represented in two dimensions or 2.5 dimensions. Wang et al. (Wang, 2018) and Monifor et al. (Moinfar et al., 2014) discussed some computational geometry issues associated with the representation of the 3D crack with arbitrary strikes and dip angles, shapes, curvatures, and connections. Hui et al. (Hui et al., 2018) introduced three types of geometrical partitioning to capture scenarios with complicated fracture-matrix topological characteristics. Thirdly, the high conductivity differences between fracture and matrix may cause convergence stability issues in numerical simulation. Hajibeygi et al. (Hajibeygi et al., 2011) developed the iterative multiscale finite volume (i-MSFV) method for EDFM to enhance the convergence performance by splitting the fully coupled system into smaller systems.

The development of EDFM enables us to conduct engineering analysis of complicated fracture-related fluid flow and heat transfer problems, e.g., numerical simulation of unconventional petroleum reservoirs and EGS geothermal reservoir with hydraulic fractures. Wang discussed a two-stage coupling strategy between the EDFM and X-FEM for the fluid flow and solid deformation coupling to simulate the fluid-driven fracture propagation process in porous media (Wang, 2018). Karvounis and Jenny introduced the adaptive hierarchical fracture model for enhanced geothermal systems and suggested the usage of kernel functions to capture fracture discontinuities (Karvounis and Jenny, 2016). Praditia et al. formulated the numerical scheme combining EDFM and single-phase flow in fractured geothermal reservoirs from scratch and conducted numerical studies on 2D conceptual cases with strong heterogeneity (Praditia et al., 2018). Vasilyeva et al. developed a method combining the unstructured fine grid approach with the generalized multiscale finite element method for EGS applications (Vasilyeva et al., 2019). However, these above numerical models may require further development in order for practical EGS applications, because equations describing fluid flow/heat transfer and relevant PVT are oversimplified. Some key features such as multiphase fluid flow, heat convection, water vaporization/condensation, well modeling, and complicated fracture geometries etc. need to be considered.

In this paper, we introduce an embedded 3D fracture modeling approach compatible with some well-established geothermal simulators, e.g. TOUGH2 technology (Pruess et al., 1999), aiming for its engineering applications in realistic HDR geothermal reservoirs. We give our novel solutions addressing two crucial technical issues for this objective. The first is a general 3D geometrical calculation algorithm to preprocess 3D hydraulic fracture geometrical information, because multiple hydraulic fractures characterized from HDR geothermal field cases cannot be represented simply in two dimensions or 2.5 dimensions, as can be observed in the following case study section. Secondly, we present a one-level LGR approach to retain simulation accuracy. Our analysis indicates that the accuracy of EDFM for heat transfer simulation is more challenging than fluid flow in the porous medium because the thermal diffusivity is typically two orders of magnitude smaller. We use a trial-and-error approach to optimize the LGR size by comparisons with analytical solutions. Then the capacity of the developed embedded 3D fracture modeling approach is demonstrated by revisiting the Fenton Hill HDR projects. This paper is organized as follows. Governing equations are briefly introduced in Section 2. In Section 3, key techniques to realize the 3D-EDFM and its accuracy evaluations are described. In Section 4, two typical problems are simulated to validate the accuracy of the developed EDFM models. In Section 5, we performed a numerical modeling study with EDFM to history match the performance of the Fenton Hill HDR projects, simulated scenarios with complicated fracture systems (both Phase 1 and Phase 2 of the Fenton Hill HDR projects), and conducted sensitivity analysis about the production temperature with respect to the injection rate, the heat conductivity, and the specific heat.

2. Governing equations

The mathematical and numerical framework starts from the integral form of mass and energy balance equations of describing fluid and heat flow in a multi-phase, multi-component system (Pruess et al., 1999; Fakcharoenphol et al., 2013):

$$\frac{d}{dt}\int_{V_n}\mathbf{M}^{\kappa}dV_n = \int_{\Gamma_n}\mathbf{F}^{\kappa}\cdot\mathbf{n}d\Gamma_n + \int_{V_n}q^{\kappa}dV_n \tag{1}$$

where V_n is an arbitrary subdomain for integration bounded by the close surface Γ_n; the quantity $\mathbf{M}$, $\mathbf{F}$, and q denote the accumulation term (mass or energy per volume), the flux term, and sink/source term, respectively; $\mathbf{n}$ is a normal vector on subdomain surface pointing inward into the element; the superscript κ represents one component, and the subscript n denotes one grid blocks.

The general form of the mass accumulation term is:

$$\mathbf{M}^{\kappa} = \sum \phi S_{\beta}\rho_{\beta}X_{\beta}^{\kappa} \tag{2}$$

where ϕ is the effective porosity, ρ_{β} is the density of phase β, S_{β} is the phase saturation, X_{β}^{κ} is the mole fraction of component κ in phase β.

The heat accumulation term consists of contributions from the rock matrix, liquid phases. It is given by equation:

$$\mathbf{M}^{\kappa} = (1-\phi)\rho_R C_R T + \phi\sum_{\beta}S_{\beta}\rho_{\beta}u_{\beta} \tag{3}$$

where ρ_R and C_R are grain density and specific heat of the host rock respectively, T is the temperature, and u_{β} is the specific internal energy in phase β.

In the mass flux term, $\mathbf{F}^{\kappa}$ is the advective mass flux summing over phases:

$$\mathbf{F}^{\kappa} = \sum_{\beta}X_{\beta}^{\kappa}\mathbf{F}_{\beta} \tag{4}$$

where $\mathbf{F}_{\beta}$ can be expressed by the multiphase extension of Darcy's law:

$$\mathbf{F}_{\beta} = -k_0\frac{k_{r\beta}\rho_{\beta}}{\mu_{\beta}}(\nabla P_{\beta} - \rho_{\beta}\mathbf{g}) \tag{5}$$

where k_0 is the absolute permeability, $k_{r\beta}$ is the relative permeability to phase β, μ_{β} is the viscosity, P_{β} is the pressure in β phase, and $\mathbf{g}$ is the vector of gravitational acceleration. Eq. (5) governs fluid flow between matrix-matrix, matrix-fracture, and fracture-fracture.

The heat flux term accounts for the conduction and advection heat transfer and is given by:

$$\mathbf{F}^{\kappa} = -\left[(1-\phi)K_R + \phi\sum_{\beta}S_{\beta}K_{\beta}\right]\nabla T + \sum_{\beta}h_{\beta}\mathbf{F}_{\beta} \tag{6}$$

where K_R is the thermal conductivity of the rock, K_{β} is the thermal conductivity of the fluid phase β, and h_{β} is the specific enthalpy of phase β.

3. EDFM

In the embedded discrete fracture method (EDFM), the interactions between fractures and its surrounding matrix are accounted via the geometrical calculation. This can be explained by the discretized form of the mass flux term in Eq. (1).

$$\int_{\Gamma_n}\mathbf{F}_{\beta}\cdot\mathbf{n}d\Gamma_n = \sum_{j\in\eta_i}(\overline{\rho}_{\beta}\lambda_{\beta})_{ij+1/2}^{n+1}\gamma_{ij}[\Phi_{\beta j}^{n+1} - \Phi_{\beta j}^{n}] \tag{7}$$

where η_i contains the set of neighbor elements to which element i is directly connected; $\Phi_{\beta j}$ denotes the potential of fluid phase β in node j; and λ_{β} is the mobility of phase β;

Table 1
Procedures to calculate 3D box and plane intersections.

Algorithm Calculating 3D Box and Plane Intersection	
1:	Process begins;
2:	Find all vertices of the intersected polygon;
3:	Check if one or more of the fracture polygon points are inside the box;
4:	Check if any of the box edges are intersected with the fracture polygon face;
5:	Check if any of the fracture polygon's edges are intersected with the box faces;
6:	Merge duplicates on the vertex list (if the plane crosses exactly the box corner);
7:	**if** (Vertex Number) > 2 **then**
8:	Sort vertices in the clockwise or counterclockwise order;
9:	Calculate the area and the average distance of the intersected polygon;
10:	**else**
11:	No effective intersection between the polygon and the box;
12:	**endif**

$$\lambda_{\beta} = \frac{k_{r\beta}}{\mu_{\beta}} \tag{8}$$

and the transmissivity of flow terms is defined as

$$\gamma_{ij} = \frac{A_{ij}k_{ij+1/2}}{d_i + d_j} \tag{9}$$

where A_{ij} is the common interface area between the intersected block and the fracture; d_i and d_j are distances from the center of each block to the common interface; $k_{ij+1/2}$ is an averaged (such as harmonic-weighted) absolute permeability.

The key to incorporate the fracture-matrix interactions through the EDFM is obtaining the contact area and the average distance between the virtually embedded fracture element and its surrounding matrix grid blocks. Such geometric calculation is straightforward for 2D or 2.5D cases, but it is challenging for 3D cases. Table 1 summarizes the key steps of the algorithm to calculate the intersection between a plane and a 3D cube. We also discussed some auxiliary techniques to handle fractures with infinite or finite conductivities, as well as multiple connected fractures.

Fig. 1 plots an illustration example of the intersection between one fracture plane and one 3D grid. In this case, the fracture polygon is partially intersected with the grid blocks. The intersection area is a quadrilateral with vertices P1, P2, P3, and P4. The vertex P4 is the fracture polygon points inside the grid box (step 3 in Table 1), P2 is the intersection between the grid edge and the fracture polygon face (step

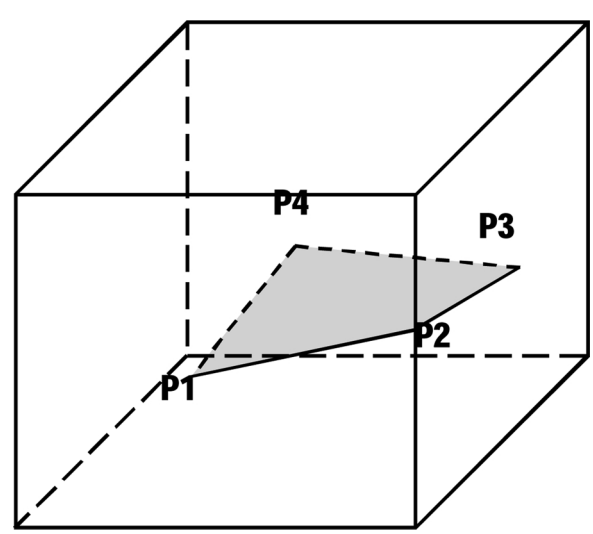

Fig. 1. Illustration of the intersection between one fracture plane and one 3D grid block.

4), and P1 and P3 are intersections between fracture polygon edges and grid faces (step 5). With the coordinate information of these vertices, the common interface area and distances from the matrix continuum block to the fracture can then be calculated for the fluid flow and heat transfer transmissivity (Wang, 2018).

The accuracy of the EDFM is evaluated by comparing its assumptions with analytical-solution based parameters. Our quantitative analysis indicates that the EDFM cannot provide solutions with unconditional accuracy. The numerical error comes from the simplification in handling local interactions between the fracture and its surrounding matrix grid blocks. For some extreme cases, this numerical error could be significant. However, we also find that this numerical error can be mitigated if the local matrix grid blocks are properly refined. We provide an analytical-solution based method to optimize this local grid refinement size if needed.

Consider governing equations for both the heat conduction and fluid flow in the porous medium, which share the following form:

$$\frac{\partial u}{\partial t} - \alpha \nabla^2 u = 0 \tag{10}$$

In the heat equation, u denotes the temperature, and α is the thermal diffusivity; in the equation describing fluid flow in the porous medium, u denotes the pressure, and α is the diffusivity. The definition of α is as follows:

$$\alpha = \begin{cases} k_t/(c_p\rho), \text{heat transfer} \\ k_f/(\phi\mu c_t), \text{fluid flow} \end{cases} \tag{11}$$

where k_t is the thermal conductivity; c_p is the specific heat capacity; ρ is the mass density of the material; k_f is the permeability; ϕ is the porosity; μ is the fluid viscosity; and c_t is the total compressibility.

We solve Eq. (10) analytically for a 1D problem with a constant fracture pressure condition (Dirichlet condition) on the right and with a closed boundary condition (Neumann condition) applied on the left (Wang, 2018; Wang et al., 2019). This analytical solution gives us an accurate evaluation of the average distance between the fracture and its surrounding matrix grid blocks, as shown in Eq. (12). The average distance in the EDFM geometrical approximated processing is given in Eq. (13).

$$d_{analytical} = \frac{x_L^2 \sum_{n=1}^{\infty} \frac{1}{(n-0.5)^2}\left(1 - \cos\left[(n-0.5)\pi\frac{\Delta x_1}{x_L}\right]\right)\exp\left[-(n-0.5)^2\pi^2\frac{\alpha}{x_L^2}\Delta t\right]}{\Delta x_1 \pi^2 \sum_{n=1}^{\infty} \exp\left[-(n-0.5)^2\pi^2\frac{\alpha}{x_L^2}\Delta t\right]} \tag{12}$$

$$d_{edfm} = \frac{\Delta x_1}{2} \tag{13}$$

where Δx_1 is the size of local grid containing the fracture; x_L is length of this 1D reservoir. From Eq. (12), the accurate (analytical-solution based) average distance depends on the grid size, time step and the diffusivity. The relative error in terms of the average distance is defined as follows:

$$Error_{\text{geometry}} = \frac{|d_{edfm} - d_{analytical}|}{d_{analytical}} \tag{14}$$

Results of this geometrical preprocessing error as a function of the diffusivity, time steps and the grid size are plotted in Fig. 2 left, in which x axis labels the logarithm of diffusivity multiplies the time step to the base 10, y axis labels the grid size, and z axis labels the relative error between two average distances. As observed in this figure, this error decreases with the decrease of the grid size, with the increase of the time step, and with the increase of the diffusivity value. This indicates the EDFM geometrical processing error can be mitigated by controlling the size of local matrix grids. For most of the practical geothermal simulation problems, the value of thermal diffusivity is in the range between $1.0 \times 10^{-5} m^2/s$ and $1.0 \times 10^{-4} m^2/s$, while the value of diffusivity regarding the fluid flow in the porous medium is in the range between $1.0 \times 10^{-4} m^2/s$ and $1.0 \times 10^{-1} m^2/s$. Because the thermal diffusivity is typically two or three orders of magnitude smaller, maintaining the accuracy of EDFM for heat transfer simulations is more challenging than simulations of fluid flow in the porous medium.

Then we conduct series of numerical tests with EDFM on the problem of unsteady-state fluid flow from a well with a single infinite-conductivity fracture (Gringarten et al., 1974), aiming to investigate how the diffusivity, time steps, and the grid size influence the accuracy of simulation results. The analytical solution for the dimensionless pressure in the well is in Eq. (15). The dimensionless pressure from the numerical simulation is in (16), and the numerical simulation relative error is defined in (17).

$$P_{wD\_analytical} = \frac{1}{2}\sqrt{\pi t_D}\left[\text{erf}\left(\frac{0.134}{\sqrt{t_D}}\right) + \text{erf}\left(\frac{0.866}{\sqrt{t_D}}\right)\right] - 0.067\text{Ei}\left(-\frac{0.018}{t_D}\right) - 0.433\text{Ei}\left(-\frac{0.750}{t_D}\right) \tag{15}$$

$$P_{wD\_edfm} = \frac{2\pi kh}{q\mu}(P_{wi} - P_{w\_edfm}) \tag{16}$$

$$Error_{numerical} = \frac{|P_{wD\_analytical} - P_{wD\_edfm}|}{P_{wD\_analytical}} \tag{17}$$

Variations of the numerical simulation error with respect to the diffusivity, time steps, and the grid size are demonstrated in Fig. 2 right, of which the trend is similar to the geometrical preprocessing error. The relationship between the numerical error and the corresponding geometrical error is plotted in Fig. 3. It's observed that these two variables are positively correlated, following an exponential-like relationship. In this way, numerical simulation errors of the EDFM can be estimated and then mitigated by adjusting the local grid size (Eq. (14)). From Fig. 3, the numerical simulation error can be retained within 10 % if the geometrical processing relative error is controlled under 0.4.

Fig. 4 plots pairs of curves on the required grid size vs. $\log_{10}(\alpha\Delta t)$ to control geometrical relative errors under given values. For example, if the diffusivity of the geothermal reservoir is $1.0 \times 10^{-3} m^2/s$, the time step in the simulation is 1000s, and the constrained geometrical relative error is 0.4, suggested LGR size will be 4 m from this figure.

4. Validations

This is to examine the accuracy of the EDFM in simulating fluid flow and heat transfer with fractures. The problem concerns fluid flow and heat transfer across a 1D vertical fracture, which is bounded by impermeable rocks. The mechanical and chemical processes are beyond the scope of this study. The system contains single-phase isothermal water at initial, and a constant water mass injection rate with a colder temperature is imposed at the inlet of the fracture. The outlet end of the fracture is kept at a constant pressure. Table 2 summarizes the parameters used in the simulation (Fig. 5).

We studied two scenarios (with or without consideration of heat supplies from surrounding rocks) with two numerical approaches. In the first approach, only fractures are included in the numerical model through an explicit approach, and the heat interaction between the fracture and its surrounding rocks is incorporated by semi-analytical solutions (Vinsome and Westerveld, 1980; Pruess and Bodvarsson, 1983; Pruess et al., 1999). In the second approach, both the fracture and its surrounding rocks are included in the numerical setup. The fracture is handled by the EDFM.

Fig. 6 presents the simulation results of the outlet temperature vs. time for these four cases. It's observed that results based on the EDFM have a good agreement with semi-analytical solutions for both scenarios. The case with no supplies of heat from surrounding rocks has an

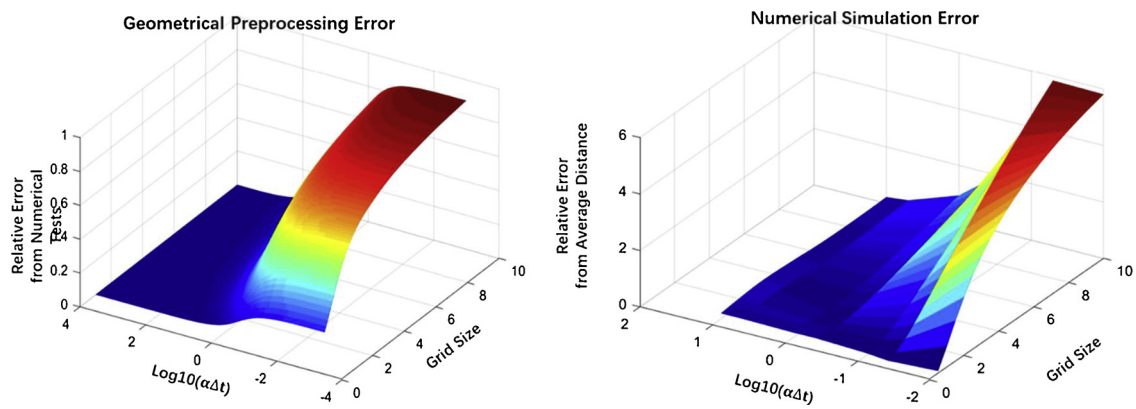

Fig. 2. Relative error of the geometric preprocessing (left) and numerical simulation (right) as a function of diffusivity, time step and grid size.

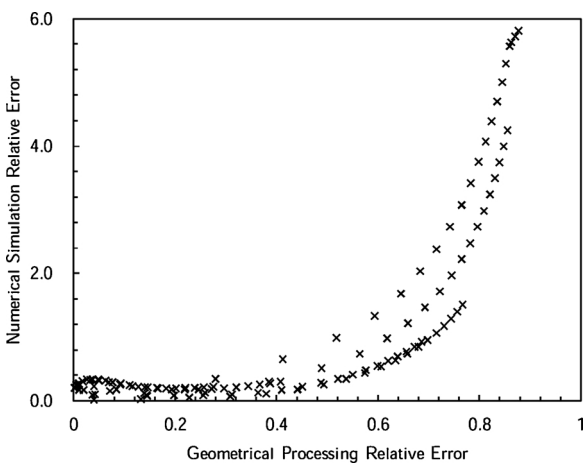

Fig. 3. Correlation between the geometrical processing error and numerical simulation error.

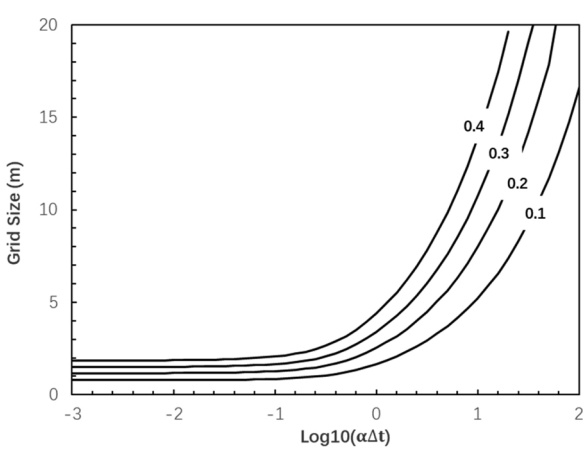

Fig. 4. Type curves for the grid size to control geometrical relative errors under given values.

early thermal breakthrough time and a following faster temperature decrease.

5. Applications

The case study in this section is based on a project initiated at the Los Alamos Scientific Laboratory to investigate the feasibility of extracting energy from the hot, dry rock. Its detailed descriptions can be referred to previous literature (Murphy, 1979; Dash et al., 1983). This project locates at Fenton Hill in the Jemez Mountains of northern New

Table 2
Parameters and values for EDFM validations.

Properties	Value	Unit
Rock		
Density	2650	kg/m^3
Heat conductivity	5.1	W/(m°C)
Specific heat	1000	J/(kg°C)
Permeability	0	m^2
Porosity	0.00	
Fracture		
Permeability	2.00E-10	m^2
Porosity	0.5	
Width	0.04	m
Initial Conditions		
Temperature	300	°C
Pressure	1.00E+07	Pa
Injection		
Temperature	100	°C
Rate	0.5	kg/s
Production		
Flowing BHP	1.00E+07	Pa

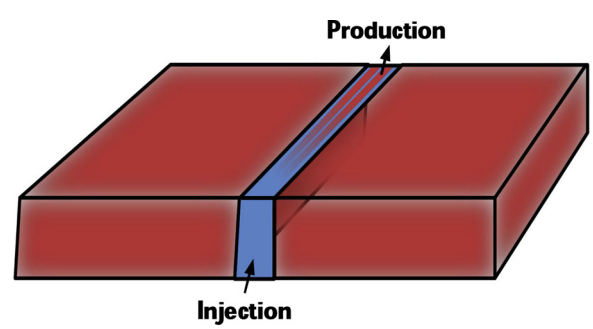

Fig. 5. Illustrations of fluid flow and heat transfer across a 1D vertical fracture.

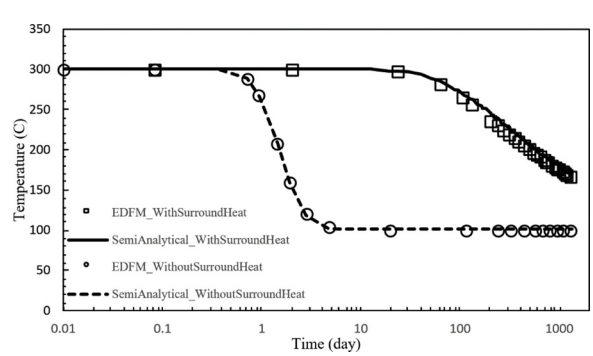

Fig. 6. The outlet temperature for two scenarios by EDFM and by the semi-analytical approach.

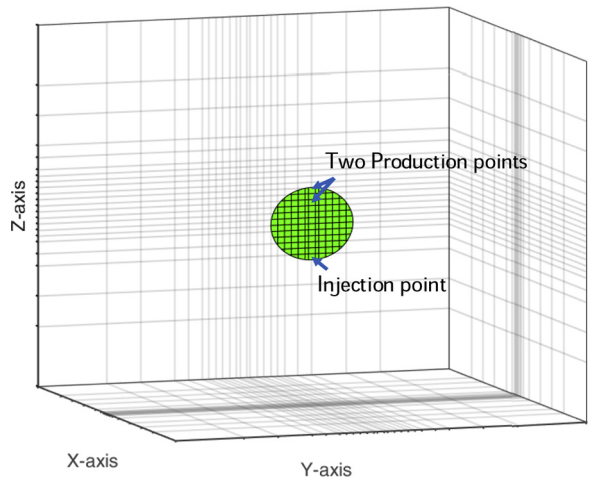

Fig. 7. Schematic review of the fracture, injection point and production points in the case study.

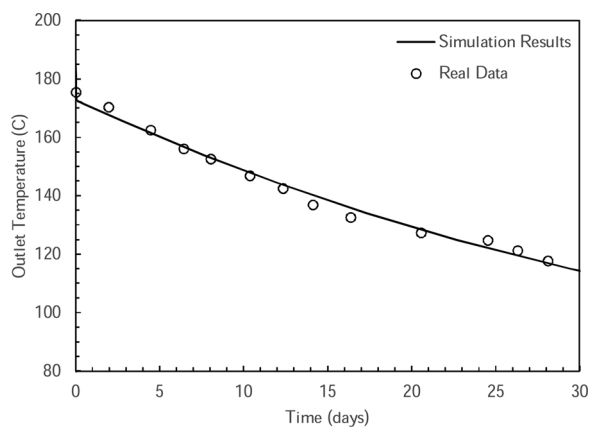

Fig. 8. History matching between the simulation result and field-recorded temperature data.

Table 3
Parameters and values in the case study.

Properties	Value	Unit
Rock		
Density	2650	kg/m^3
Heat conductivity	3.9	W/(m°C)
Specific heat	750	J/(kg°C)
Permeability	0	m^2
Porosity	0.00	
Fracture		
Permeability	2.00E-10	m^2
Porosity	0.5	
Width	0.002	m
Radius	60	m
Initial Conditions		
Temperature	190	°C
Pressure	1.00E+07	Pa
Injection		
Temperature	25	°C
Rate	7.5	kg/s
Production		
Flowing BHP	1.00E+07	Pa

Mexico. In phase one of the project, a geothermal reservoir is formed by hydraulic fracturing a hot, non-porous granite at 2.81 km in depth. Since the granitic rock is relatively homogeneous and unstratified, the hydraulic fracture can be assumed to be approximately circular in shape. The temperature at this site is 197 °C, with a geothermal heat

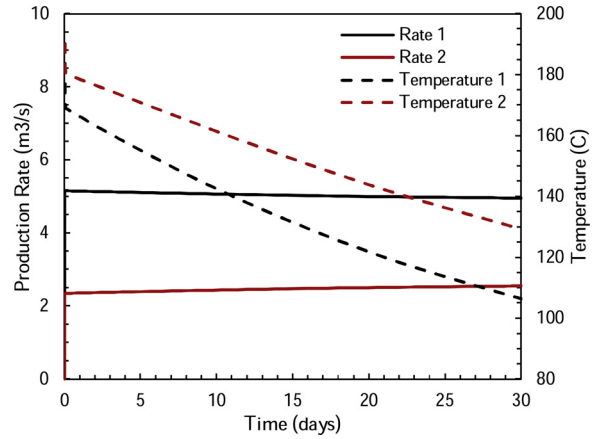

Fig. 9. Production rates and temperatures at two outlets.

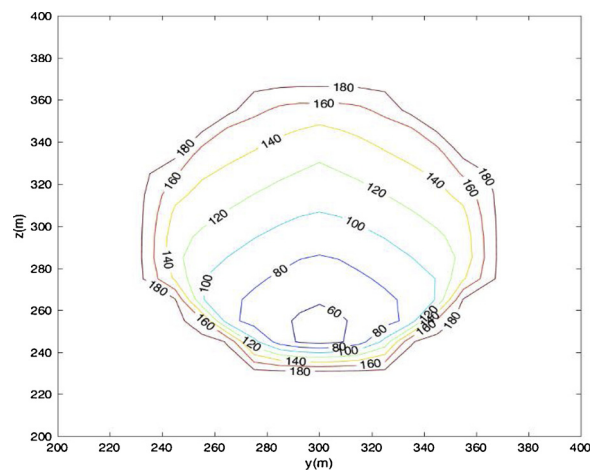

Fig. 10. Temperature contour inside the fracture after injection of 30 days.

flow of 0.16 W/m^2 (2.5 times the world average). The circulation loop is created by drilling two wells (one injection well and one production well) intersecting the hydraulic fracture region, and the fracture acts as the flow short-circuit between the injection and production wells. The injection point is located at the bottom of the fracture. The production well connects with two existing points inside the fracture at the shallower depth according to the temperature and radioactive tracer surveys. This injection/production system is schematically illustrated in Fig. 7. The water alone, with no additives or propping agents, are used to extract heat from this reservoir by the heat conduction when the water is exposed to hot rock surfaces. Because the surrounding granite rocks are almost non-porous and impermeable, less than 1% of the injected water is lost outside the fracture.

Injection flow rates and production temperatures were measured by surveying tools. Fig. 8 presents the recorded temperature variation with time in the production well for the first 30 days. The corresponding injection flow rate keeps constant at $7.5\times10^{-3}m^3/s$. We performed a numerical modeling study to history match the performance of this geothermal reservoir. In the basic model setup, the reservoir is assumed to be rectangular with dimensions of 600 m× 600 m× 600m. Though a realistic reservoir extent may be larger, we considered it appropriate to simplify calculations by modeling a smaller domain of only 600 m in vertical and lateral extent. The computational mesh is three-dimensional and contains 19 × 23 × 22 grid blocks, which are nonuniform with refinement around the fracture edge to capture the fracture geometry (Fig. 7. The circular fracture is embedded into the original grids, leading to 9758 computational grids 9614 matrix grids and 144 fracture grids, and 27,888 computational connections 27,481 matrix-matrix

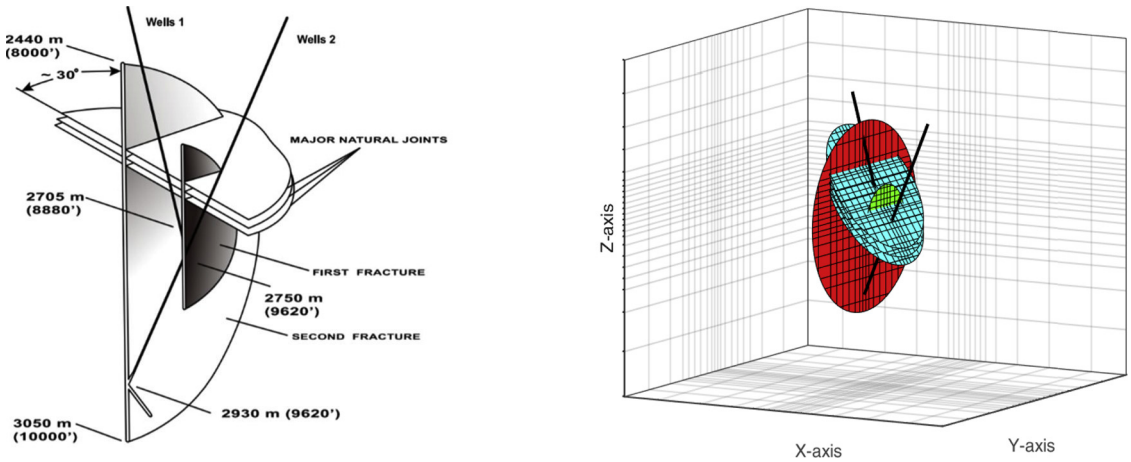

Fig. 11. Intepreted fracture geometry from previous studies (modified from Dash et al., 1983) and the numerical implementation by EDFM.

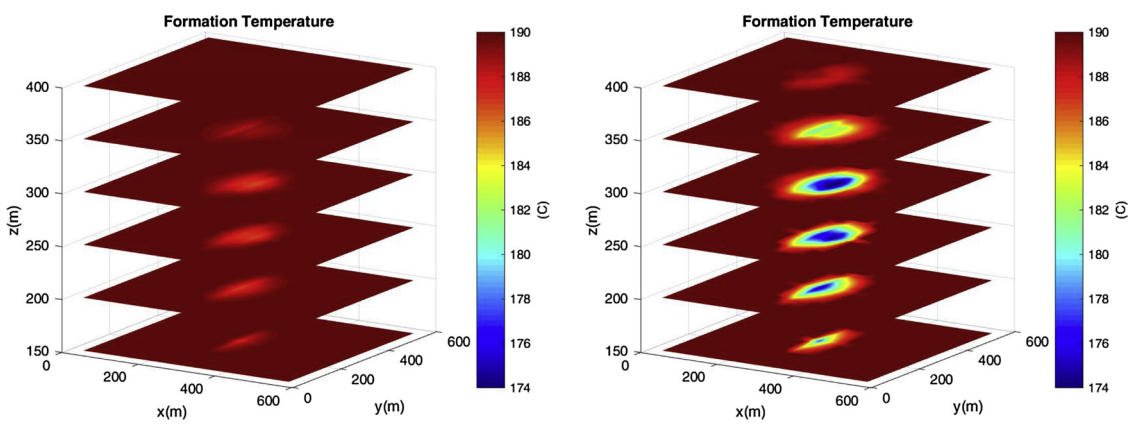

Fig. 12. Temperature distributions in formations at 1 month and 1 year.

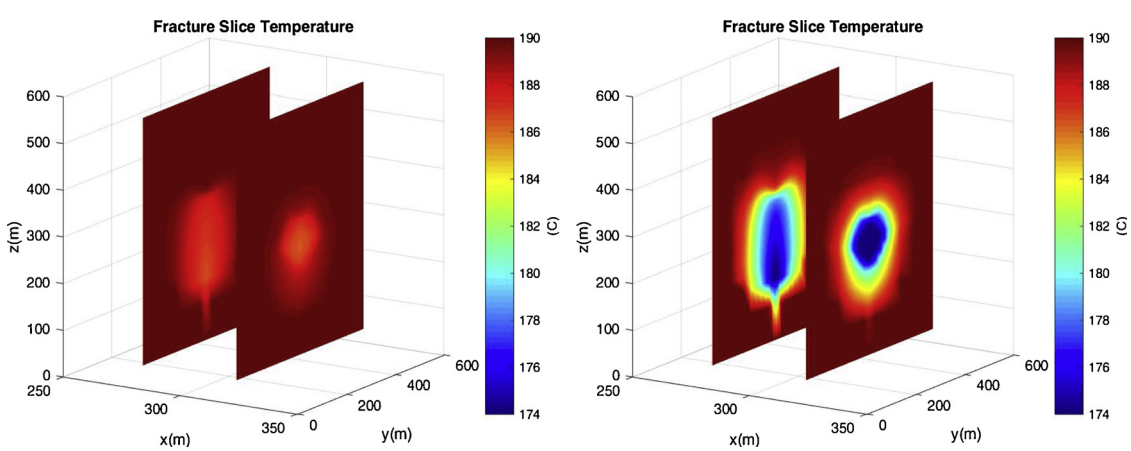

Fig. 13. Temperature distributions in fractures at 1 month and 1 year.

connections, 144 matrix-fracture connections, and 263 fracture-fracture connections. In this history matching, three sets of adjustable parameters were used: the fracture radius, the fracture width, and the injection temperature. These parameters were adjusted until simulation results matched observed production temperature data. Table 3 summarizes the parameters used in the simulations for the final match. As demonstrated in Fig. 8, simulation results of the case with a fracture radius of 60 m, the fracture aperture of 0.002 m and the injection temperature of 25 °C agree remarkably well with the field recorded data. The temperature of the production rate declines rapidly in this case. It takes 30 days for the temperature to decrease from 175 °C to 114 °C. Parameter values from this history matching are close to previous characterizations of this geothermal reservoir as described in the literature.

Fig. 9 plots simulated production rates and production temperatures from these two outlets. The first outlet (the one close to the injection point) transmits approximately 70 % of the flow, while the second transmits about 30 %. The temperature of the production fluids drops faster in the first outlet. The mixed-mean fluid temperature, required for comparisons with measurements, is calculated as the sum of the product of the flow fraction and the computed temperature for the positions corresponding to the two communicating joints. Fig. 10 plots

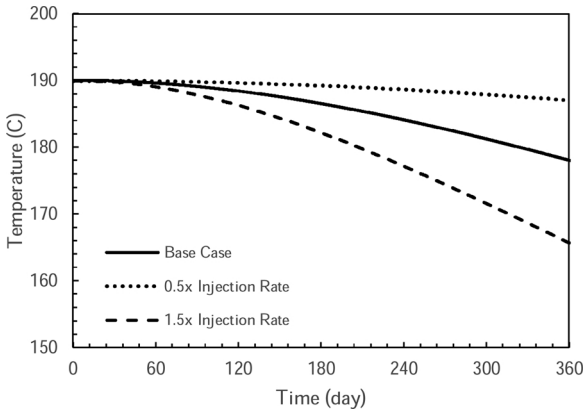

Fig. 14. Sensitivity analysis of the production temperature with respect to the injection rate.

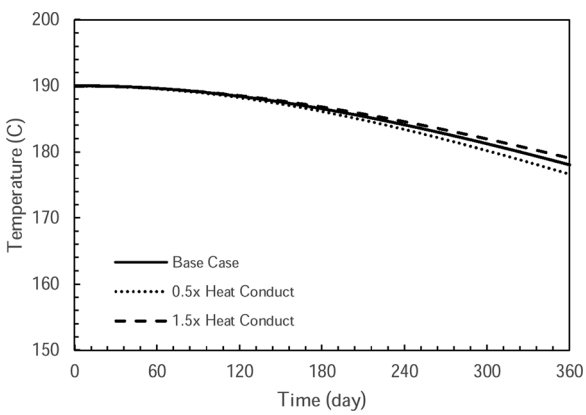

Fig. 15. Sensitivity analysis of the production temperature with respect to the heat conductivity.

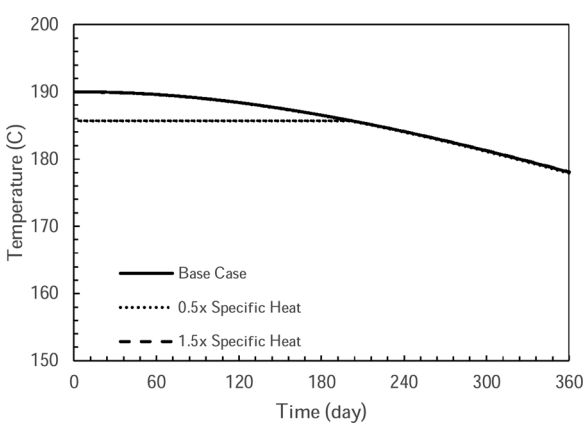

Fig. 16. Sensitivity analysis of the production temperature with respect to the specific heat.

the temperature contour inside this fracture after 30 days.

Next, we simulate the same geothermal reservoir with a more complicated fracture system as characterized from the phase 2 of the Fenton Hill HDR geothermal project (Dash et al., 1983). The fracture system is enlarged by extending another vertical hydraulic fracture. These two vertical hydraulic fractures are connected by three non-vertical natural fractures with a dip of about 60° from horizontal. The effective heat-transfer area is thus significantly increased by considering both the second hydraulic fracture and natural fractures. The fracture geometry is interpreted conceptually from previous studies. Its numerical implementation through the EDFM is illustrated in the right part of Fig. 11. All other reservoir properties keep the same as the one described above. Figs. 12 and 13 show the simulated temperature distribution at one month and one year in formations (horizontal slices) and in two vertical hydraulic fractures (vertical slices), respectively. Simulation results reveal our physical understandings qualitatively. The temperature in the inner reservoir part (the portion between two vertical fractures) drops faster than that in the outer reservoir part.

We further conducted six other numerical tests to investigate the sensitivity of production temperature with respect to the injection rate, the heat conductivity, and the specific heat. These three parameters are chosen because their quantitative impacts on the production temperature are of interest to improve geothermal reservoir management, while they are not straightforward from qualitative analysis. The results from the sensitivity analysis are presented in Figs. 14–16. It indicates that the injection rate has the most significant impact among these three variables on production temperature. The impact of the heat conductivity on the production temperature is slight. Increasing or decreasing the heat conductivity by 50 % only leads to about 1.5 % change in the production temperature. The impact of the specific heat on the production temperature is negligible.

6. Conclusions

We describe an efficient modeling approach, named embedded discrete fracture method (EDFM), for incorporating arbitrary 3D, discrete fractures, such as hydraulic fractures or faults, into modeling fracture-dominated fluid flow and heat transfer in fractured geothermal reservoirs. Compared with other fracture modeling approaches, it avoids cumbersome 3D unstructured, local refining procedures, and increases computational efficiency by simplifying Jacobian matrix size and sparsity, while keeps sufficient accuracy. Several numeral simulations are present to demonstrate the utility and robustness of the proposed technique. Our numerical experiments show that this approach captures all the key patterns about fluid flow and heat transfer dominated by fractures in these cases. Thus, this approach is readily available to the simulation of fractured geothermal reservoirs with both artificial and natural fractures.

Author Statement

All authors certify that they have participated sufficiently in the work to take public responsibility for the content, including participation in the concept, design, analysis, writing, or revision of the manuscript.

All co-authors have seen and agree with the contents of the manuscript. We certify that the submission is original and is not under review at any other publication.

Declaration of Competing Interest

The authors declare that they have no known competing financial interests or personal relationships that could have appeared to influence the work reported in this paper.

Acknowledgments

This work was supported in part by EMG Research Center in the Petroleum Engineering Department at Colorado School of Mines; and by Foundation CMG. Also, a portion of this research was supported by the U.S. Department of Energy, Office of Energy Efficiency and Renewable Energy (EERE), Geothermal Technologies Office (GTO) under Contract No.DE-AC36-08-GO28308 with the National Renewable Energy Laboratory as part of the EGS Collab project.

References

Computer Modeling Group Ltd, 2012. CMG-STARS User's Guide. January. .
Dash, Z.V., Murphy, H.D., Aamodt, R.L., Aguilar, R.G., Brown, D.W., Counce, D.A., Fisher,

H.N., et al., 1983. Hot dry rock geothermal reservoir testing: 1978 to 1980. J. Volcanol. Geothermal Res. Geothermal Energy of Hot Dry Rock 15 (1), 59–99. https://doi.org/10.1016/0377-0273(83)90096-3.

DeBaun, D., Byer, T., Childs, P., Chen, J., Saaf, F., Wells, M., Liu, J., Cao, H., Pianelo, L., Tilakraj, V., Crumpton, P., 2005. An extensible architecture for next generation scalable parallel reservoir simulation. January. SPE Reservoir Simulation Symposium. Society of Petroleum Engineers.

Duguid, J.O., Lee, P.C.Y., 1977. Flow in fractured porous media. Water Resour. Res. 13 (3), 558–566. https://doi.org/10.1029/WR013i003p00558.

Fakcharoenphol, Perapon, Xiong, Yi, Hu, Litang, Winterfeld, Philip H., Xu, Tianfu, Yu-Shu, Wu., 2013. User's Guide of Tough2-Egs. a Coupled Geomechanical and Reactive Geochemical Simulator for Fluid and Heat Flow in Enhanced Geothermal Systems Version 1.0. DOE-CSM–0002762-1. Colorado School of Mines, Golden, CO (United States). https://doi.org/10.2172/1136243.

Gong, B., Karimi-Fard, M., Durlofsky, L.J., 2008. Upscaling discrete fracture characterizations to dual-porosity, dual-permeability models for efficient simulation of flow with strong gravitational effects. Spe J. 13 (1), 58–67.

Gringarten, A.C., Ramey Jr., H.J., Raghavan, R., 1974. Unsteady-state pressure distributions created by a well with a single infinite-conductivity vertical fracture. Old Spe J. 14 (4), 347–360.

Hajibeygi, H., Karvounis, D., Jenny, P., 2011. A hierarchical fracture model for the iterative multiscale finite volume method. J. Comput. Phys. 230 (24), 8729–8743.

Hui, M.H.R., Mallison, B.T., Lim, K.T., 2008. An innovative workflow to model fractures in a giant carbonate reservoir. January In: International Petroleum Technology Conference. International Petroleum Technology Conference.

Hui, M.H.R., Karimi-Fard, M., Mallison, B., Durlofsky, L.J., 2018. A general modeling framework for simulating complex recovery processes in fractured reservoirs at different resolutions. Spe J. 23 (2), 598–613.

Karimi-Fard, M., Durlofsky, L.J., Aziz, K., 2003. An efficient discrete fracture model applicable for General purpose Reservoir simulators. Society of Petroleum Engineers. https://doi.org/10.2118/79699-MS.

Karimi-Fard, M., Gong, B., Durlofsky, L.J., 2006. Generation of Coarse-scale Continuum Flow Models From Detailed Fractured Characterizations.

Karvounis, D.C., Jenny, P., 2016. Adaptive hierarchical fracture model for enhanced geothermal systems. Multiscale Model. Simul. 14 (1), 207–231.

Kazemi, H., 1969. Pressure transient analysis of naturally fractured reservoirs with uniform fracture distribution. Old Spe J. 9 (4), 451–462. https://doi.org/10.2118/2156-A.

Lee, S.H., Lough, M.F., Jensen, C.L., 2001. Hierarchical modeling of flow in naturally fractured formations with multiple length scales. Water Resour. Res. 37 (3), 443–455. https://doi.org/10.1029/2000WR900340.

Moës, N., Dolbow, J., Belytschko, T., 1999. A finite element method for crack growth without remeshing. Int. J. Numer. Methods Eng. 46 (1), 131–150.

Moinfar, A., Varavei, A., Sepehrnoori, K., Johns, R.T., 2014. Development of an Efficient Embedded Discrete Fracture Model for 3D Compositional Reservoir Simulation in Fractured Reservoirs. Spe J. 19 (2), 289–303. https://doi.org/10.2118/154246-PA.

Murphy, H.D., 1979. Heat production on from a geothermal Reservoir formed By hydraulic fracturing - comparison of Field and theoretical results. Society of Petroleum Engineers. https://doi.org/10.2118/8265-MS.

Praditia, T., Helmig, R., Hajibeygi, H., 2018. Multiscale formulation for coupled flow-heat equations arising from single-phase flow in fractured geothermal reservoirs. Comput. Geosci. 22 (5), 1305–1322.

Pruess, K., Bodvarsson, G.S., 1983. Thermal Effects of Reinjection in Geothermal Reservoirs With Major Vertical Fractures. No. LBL-16269; CONF-8310121-7. Lawrence Berkeley Lab., CA (USA).

Pruess, K., Schroeder, R.C., 1980. "Shaft79 User's Manual." LBL-10861. California Univ. Lawrence Berkeley Lab, Berkeley (USA). https://doi.org/10.2172/5355427.

Pruess, K., Wu, Y.S., 1988. On Pvt-Data, Well Treatment, and Prepartion of Input Data for an Isothermal Gas-Water-Foam Version of Mulkom. LBL-25783. Lawrence Berkeley Lab., CA (USA). https://www.osti.gov/scitech/biblio/6121230.

Pruess, Karsten, Oldenburg, C.M., Moridis, G.J., 1999. TOUGH2 User's Guide Version 2. Lawrence Berkeley National Laboratory. http://escholarship.org/uc/item/4df6700h.pdf.

Sadrpanah, H., Charles, T., Fulton, J., 2006. Explicit simulation of multiple hydraulic fractures in horizontal Wells. Society of Petroleum Engineers. https://doi.org/10.2118/99575-MS.

SCHLUMBERGER, 2009. ECLIPSE User Manual. Technical Description. Schlumberger Ltd.

Settari, A., Walters, D.A., 2001. Advances in Coupled Geomechanical and Reservoir Modeling With Applications to Reservoir Compaction. Spe J. 6 (3), 334–342. https://doi.org/10.2118/74142-PA.

Slough, K.J., Sudicky, E.A., Forsyth, P.A., 1999. Grid refinement for modeling multiphase flow in discretely fractured porous media. Adv. Water Resour. 23 (3), 261–269. https://doi.org/10.1016/S0309-1708(99)00009-3.

Sun, J., Schechter, D.S., 2014. Optimization-based unstructured meshing algorithms for simulation of hydraulically and naturally fractured reservoirs with variable distribution of fracture aperture, spacing, length and strike. Society of Petroleum Engineers. https://doi.org/10.2118/170703-MS.

Ţene, M., Bosma, S.B., Al Kobaisi, M.S., Hajibeygi, H., 2017. Projection-based embedded discrete fracture model (pEDFM). Adv. Water Resour. 105, 205–216.

Vasilyeva, M., Babaei, M., Chung, E.T., Spiridonov, D., 2019. Multiscale modeling of heat and mass transfer in fractured media for enhanced geothermal systems applications. Appl. Math. Model. 67, 159–178.

Vinsome, P.K.W., Westerveld, J., 1980. A Simple Method For Predicting Cap And Base Rock Heat Losses In' Thermal Reservoir Simulators. J. Can. Pet. Technol. 19 (3). https://doi.org/10.2118/80-03-04.

Wang, C., 2018. Multi-scale, Multi-continuum and Multi-physics Model to Simulate Coupled Fluid Flow and Geomechanics in Shale Gas Reservoirs, A. PhD Diss. Colorado School of Mines. Arthur Lakes Library.

Wang, C., Ran, Q., Wu, Y.-S., 2019. Robust implementations of the 3D-EDFM algorithm for reservoir simulation with complicated hydraulic fractures. J. Pet. Sci. Eng. 181, 106229.

Warren, J.E., Root, P.J., 1963. The behavior of naturally fractured reservoirs. Old Spe J. 3 (3), 245–255. https://doi.org/10.2118/426-PA.

Wu, Y.-S., Ehlig-Economides, C., Qin, Guan, Kang, Zhijang, Zhang, Wangming, Ajayi, Babatunde, Tao, Qingfeng, 2007. A Triple-Continuum Pressure-Transient Model for a Naturally Fractured Vuggy Reservoir. August. Lawrence Berkeley National Laboratory. http://escholarship.org/uc/item/8fr0m0pp.